Earth Planets Space, **57**, 15–28, 2005

Influence of lattice thermal conductivity on thermal convection with strongly temperature-dependent viscosity

Tomohiko K. B. Yanagawa[1], Masao Nakada[2], and David A. Yuen[3]

[1]*Department of Earth and Planetary Sciences, Graduate School of Sciences, Kyushu University, 6-10-1 Hakozaki, Fukuoka 812-8581, Japan*
[2]*Department of Earth and Planetary Sciences, Faculty of Science, Kyushu University, 6-10-1 Hakozaki, Fukuoka 812-8581, Japan*
[3]*Department of Geology and Geophysics, University of Minnesota Supercomputing Institute, University of Minnesota, Minneapolis, MN 55455-0219, U.S.A.*

(Received June 14, 2004; Revised December 3, 2004; Accepted December 10, 2004)

To examine the effects of temperature-dependent lattice thermal conductivity (lattice-k) on the thermal convection with a temperature-dependent viscous fluid, particularly on the upper thermal boundary layer, we have studied numerically 2-D thermal convective flows with both constant thermal conductivity (constant-k) and lattice-k models. Numerical experiments with large viscosity contrasts, greater than a million, produce a cooler and thinner upper thermal boundary layer for the lattice-k compared with those for the constant-k, implying that thermal convection with lattice-k produces a much sharper boundary between the lithosphere and asthenosphere. The differences between the constant-k and lattice-k can be reasonably explained by the following two causes: (i) the decreasing lattice-k with depth increases an effective Rayleigh number around the bottom of the thermal boundary layer, and (ii) the distribution of lattice-k and uniform vertical heat flux within the thermal boundary layer determine the temperature distribution. The predicted sharper boundary, i.e. sharper vertical viscosity gradient near the bottom of the lithosphere, may play an important role on controlling the amount of lithospheric deformation associated with the downwelling.
Key words: Mantle convection, lattice thermal conductivity, variable viscosity.

1. Introduction

Recently, Hofmeister (1999, 2001) has proposed a new semi-empirical thermal conductivity model based on solid-physics to account for the temperature- and pressure-dependent thermal conductivities of mantle materials. Some studies of thermal convection with variable thermal conductivity based on Hofmeister's model have been carried out in applications of mantle convection (Dubuffet *et al*., 1999, 2000b, 2002; Dubuffet and Yuen, 2000a; van den Berg *et al*., 2001, 2002a; van den Berg *et al*., 2002b). They found some interesting results, for example, the changes in thickness of plumes (Dubuffet and Yuen, 2000; Dubuffet *et al*., 2000), in the efficiency of heat transfer (van den Berg *et al*., 2001, 2002) and in the stability near the core-mantle boundary (CMB) (Dubuffet *et al*., 2002). Yanagawa *et al*. (2004) have also studied the effects of depth-dependent thermal conductivity by using simplified stratifications of thermal conductivity. They found that actual values of thermal conductivity in top and bottom thermal boundary layers exert significant effects on volumetrically averaged temperature, velocity and heat flux of thermal convection compared with those in the interior between both thermal boundary layers (TBLs). They also found that averaged value of thermal conductivity for each layer is more important than vertical profile of thermal conductivity in each layer. However, all of these models have not included the effects of variable viscosity, which evidently play an important role in mantle convection (e.g. Weinstein and Christensen, 1991; Tackley, 1993; Solomatov, 1995). Therefore it may be difficult to apply their constant viscosity results to the mantle.

In this paper, we set out to study mantle convection with both a temperature-dependent viscosity and temperature-dependent thermal conductivity. Thermal conductivity can be divided into two components with different physics, i.e. the components of lattice conduction, and of radiation (Schatz and Simmons, 1972). The lattice contribution decreases rapidly with increasing temperature, especially at low temperatures, as expected for the lithosphere, for example, $T < 1440$ K for depth above 70 km (Schatz and Simmons, 1972; Hofmeister, 1999). On the other hand, the radiative contribution increases rapidly with increasing temperature, especially at high temperatures, for example, $T > 1870$ K for depth below 670 km (Schatz and Simmons, 1972; Hofmeister, 1999; Clark, 1957). The temperature-dependent viscosity also decreases exponentially as temperature increases (Frank-Kamenetskii, 1969), and the various viscosity contrasts across the layer produce some distinct kinds of patterns in mantle convection. The dynamical behavior of the lithosphere especially depends on the viscosity contrast across the layer (Solomatov, 1995; Solomatov and Moresi, 1997; Kameyama and Ogawa, 2000).

The temperature-dependent lattice thermal conductivity plays important roles on the thermal history of the plan-

ets and on the dynamics of the thermal boundary layers, particularly on the dynamics of the lithosphere discussed here. Yanagawa *et al*. (2004) mainly investigated the former point based on a simple depth-dependent, layered thermal conductivity model, and found that decreasing thermal conductivity with depth causes a weakened convection. We also examine this point here. In this study, however, we mainly examine the effects of interactions between temperature-dependent lattice thermal conductivity and temperature-dependent viscosity on the dynamics of the lithosphere, and compare them with the results obtained by Solomatov (1995) and Kameyama and Ogawa (2000). In Section 2, we introduce two-dimensional (2D) models with variable viscosity and lattice thermal conductivity, and then describe the results with both temperature-dependent viscosity and thermal conductivity in Section 3. In Section 4, we summarize the results and apply them to other planetary interiors.

2. Model Description

We consider thermal convection of Newtonian fluid with strongly temperature-dependent viscosity and temperature-dependent thermal conductivity in a 2D rectangular box. A temperature difference between the top and bottom boundaries is fixed. Free-slip condition is imposed on the horizontal boundaries and the lateral boundaries are reflective. The following assumptions are imposed on the fluid; (1) the fluid is incompressible, (2) the Prandtl number is infinite, (3) no mechanical heating is included and the Boussinesq approximation is therefore valid.

The governing non-dimensional equations are derived from the conservation of mass, momentum and energy (e.g. Schubert *et al*., 2001):

$$\left(\frac{\partial^2}{\partial y^2}-\frac{\partial^2}{\partial x^2}\right)\nu(T)\left(\frac{\partial^2}{\partial y^2}-\frac{\partial^2}{\partial x^2}\right)\psi + 4\frac{\partial^2}{\partial x\partial y}\nu(T)\frac{\partial^2}{\partial x\partial y}\psi = -Ra_s\frac{\partial T}{\partial x} \quad (1)$$

$$\frac{\partial T}{\partial t} = -\left(\frac{\partial T}{\partial x}\frac{\partial \psi}{\partial z}-\frac{\partial T}{\partial z}\frac{\partial \psi}{\partial x}\right)+\nabla\cdot(\kappa(T)\nabla T) \quad (2)$$

where $T(x,z,t)$ is the temperature field and $\psi(x,z,t)$ is the stream function satisfying the conservation of mass automatically. x and z denote the horizontal and vertical coordinates respectively with z positive downwards, and t denotes time, which has been non-dimensionalized by the thermal diffusion time scale. Ra_s is the Rayleigh number based on surface property values defined at the top ($z=0$), as expressed in Eq. (5). The second term in Eq. (2) is the advection term. $\nu(T)$ and $\kappa(T)$ are non-dimensional temperature-dependent kinematic viscosity and thermal diffusivity normalized by the surface value, respectively. Thermal diffusivity κ is proportional to thermal conductivity k, $\kappa(T)=k(T)/\rho_0 c$, where ρ_0 is the reference density and c is the specific heat.

The viscosity adopted in this study, $\mu(T)=\rho_0\nu(T)$, decreases exponentially with increasing temperature;

$$\nu(T)=\frac{\mu(T)}{\rho_0}=\frac{\mu_s}{\rho_0}\exp[-\beta(T-T_s)] \quad (3)$$

where μ_s and T_s are the viscosity and temperature at the top boundary, and β is a constant controlling the viscosity contrast across the layer. The exponential formula of temperature-dependent viscosity expressed as Eq. (3) is called as the Frank-Kamenetskii approximation (Frank-Kamenetskii, 1969). Here we call the kinematic viscosity ν as the viscosity.

The lattice thermal conductivity decreases as temperature increases (Fujisawa *et al*., 1968; Kanamori *et al*., 1968). The relationship between thermal conductivity and temperature is derived by simplifying the lattice component proposed by Hofmeister (1999) and takes a following power-law form:

$$k(T)=k_s\left(\frac{T_s}{T_s+T}\right)^a \quad (4)$$

where k_s is the thermal conductivity at the top, and a is a constant associated with the type of chemical bonding in mantle minerals (Hofmeister, 1999). T_s and a are fixed at 0.1 and 0.9, respectively. The temperature-dependent lattice thermal conductivity defined by Eq. (4) is referred to as lattice-k here. In this study we have neglected the radiative thermal conductivity, which is more important for the lower mantle.

We adopt two non-dimensional parameters to understand the physics in the problem, i.e. the Rayleigh number estimated on the top Ra_s and the viscosity contrast γ_ν between the top and bottom;

$$Ra_s=\frac{\rho_0 g\alpha(T_b-T_s)d^3}{\kappa_s\mu_s} \quad (5)$$

$$\gamma_\nu=\exp[-\beta(T_b-T_s)] \quad (6)$$

where index "b" means the value evaluated at the bottom. g is the gravitational acceleration, α is the coefficient of thermal expansion and d is a thickness of the box.

The basic equations are discretized by the central finite-difference method in the diffusion term and the Arakawa-Jacobian method in the advection term (Arakawa, 1966). For a box with aspect ratio fixed at one, the numbers of vertical and horizontal grid points are 257 and 257, respectively. The energy equation is discretized by the Euler method in time. The momentum equations with temperature-dependent viscosity are solved by an iterative method, i.e. Multigrid preconditioned conjugate gradient method (Tatebe, 1993). The accuracy of results is verified by a benchmark comparison with the results of Christensen (1984). In all models, the initial condition is motionless and has an isotherm at $T=1$ with a very small disturbance in the center of the box. All models have been integrated until the volumetrically averaged temperature becomes almost steady.

3. Results

3.1 Previous works

Before discussing structures of thermal convection with interactions between both temperature-dependent viscosity and temperature-dependent thermal conductivity, we examine the convective structures of thermal convection with temperature-dependent viscosity and constant thermal conductivity (constant-k). These convective patterns

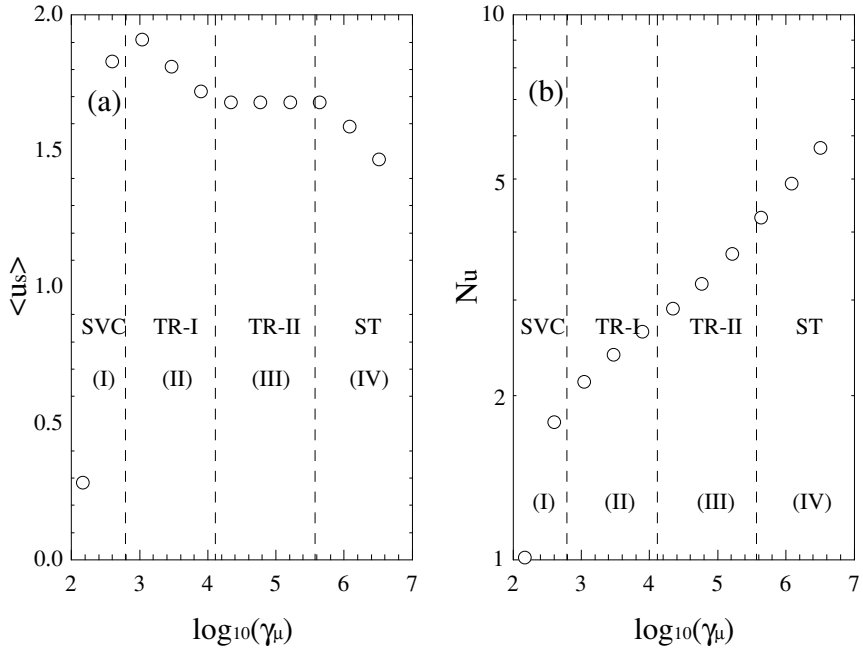

Fig. 1. Averaged horizontal velocities estimated at the top $\langle u_s \rangle$ and Nusselt number Nu versus the viscosity contrast across the layer γ_ν for models with constant-k and temperature-dependent viscosity ν. The Rayleigh number estimated at the surface Ra_s equals to 10^2, and the aspect ratio is fixed at one. The dotted lines represent the boundaries of four convective regimes, area-I, II, III and IV, i.e. the small viscosity contrast regime (SVC), the traditional regime (TR-I, TR-II) and the stagnant-lid regime (ST).

have extensively been studied, and it has been known that temperature-dependent viscosity promotes the upper TBL to be stiffer-lid as viscosity contrast across the layer increases (Weinstein and Christensen, 1991). Solomatov (1995) carried out a simple scaling analyses of thermal convection with temperature-dependent viscosity and constant-k, and predicted three convective regimes, i.e. the small viscosity contrast regime without stiff-lid (SVC), the transitional regime with a less stiff-lid (TR) and the stagnant-lid regime with a stiff-lid (ST). Moresi and Solomatov (1995) confirmed the prediction of Solomatov (1995) by carrying out 2D numerical experiments with aspect ratio fixed at one. Kameyama and Ogawa (2000) carried out 2D numerical experiments with longer horizontal scales than those by Moresi and Solomatov (1995), and found similar convective regimes.

3.2 Convective regimes for temperature-dependent viscosity and constant thermal conductivity

Figure 1 shows the averaged horizontal velocity at the surface $\langle u_s \rangle$ and Nusselt number Nu versus the viscosity contrast across the layer γ_ν. The parameters used for these numerical experiments are shown in Table 1. The average horizontal velocity $\langle u_s \rangle$ for models with aspect ratio fixed at one is defined by

$$\langle u_s \rangle = \int_0^1 u_s dx \tag{7}$$

The plot of $\langle u_s \rangle$ can be divided into four areas from the gradients; the area-I (SVC) where the viscosity contrast γ_ν is under $10^{2.6}$ and $\langle u_s \rangle$ increases as γ_ν increases, the area-II (TR-I) where γ_ν is from $10^{3.04}$ to $10^{3.9}$ and $\langle u_s \rangle$ decreases as γ_ν increases, the area-III (TR-II) where γ_ν is from $10^{4.34}$ to $10^{5.21}$ and $\langle u_s \rangle$ keeps almost constant, and the area-IV (ST) where γ_ν is over $10^{5.64}$ and $\langle u_s \rangle$ decreases as γ_ν increases. The plot of Nu can be also divided into four regimes from the gradients, although the boundary between the TR-I and TR-II is less distinct.

Table 1. The list of numerical experiments with the aspect ratio fixed at one. The Rayleigh number estimated at the surface Ra_s is equals to 10^2.

β in Eq. (3)	$\log_{10}(\gamma_\nu)$	constant-k	lattice-k
15	6.51	A-C15	A-L15
14	6.08	A-C14	A-L14
13	5.64	A-C13	A-L13
12	5.21	A-C12	A-L12
11	4.77	A-C11	A-L11
10	4.34	A-C10	A-L10
9	3.90	A-C09	A-L09
8	3.47	A-C08	A-L08
7	3.04	A-C07	A-L07
6	2.60	A-C06	A-L06
5	2.17	A-C05	A-L05
4	1.73	none	A-L04
3	1.30	none	A-L03
2	0.86	none	A-L02
1	0.43	none	A-L01

To distinguish the differences among these four regimes, we examine their convective structures by taking account of distribution of normalized viscous dissipation $\Phi/\Phi_{\rm ave}$. Viscous dissipation Φ and normalized viscous dissipation

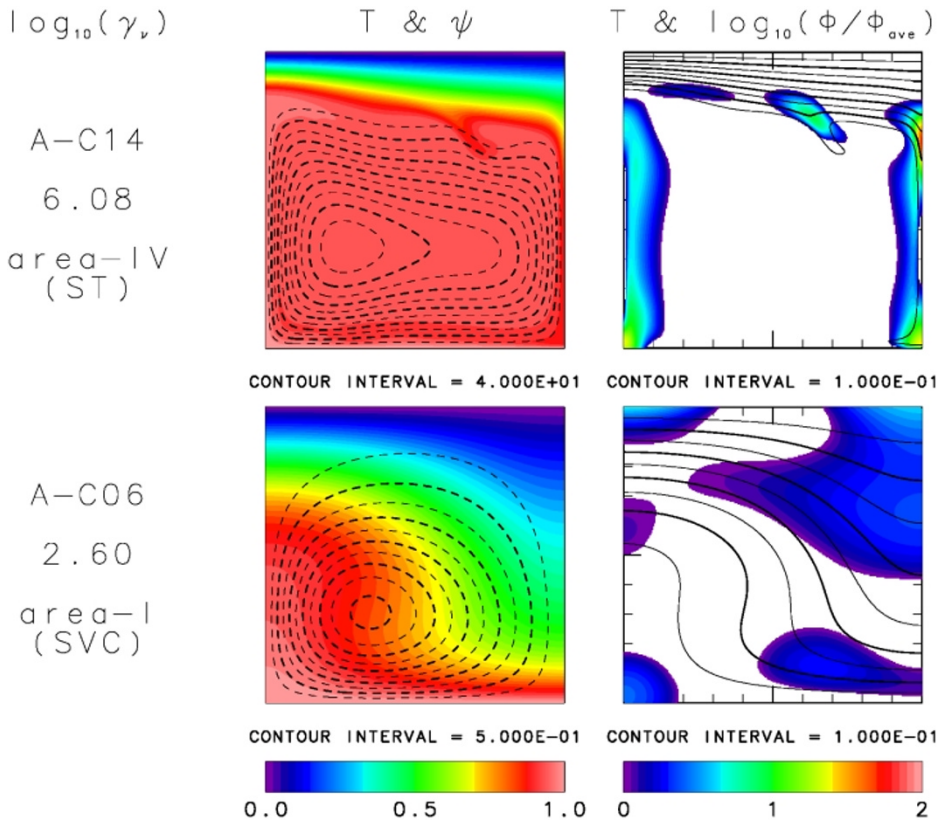

Fig. 2. Two-dimensional structures of temperature T, stream function ψ and normalized viscous dissipation $\Phi/\Phi_{\rm ave}$ for models A-C14 and A-C06 with constant-k and temperature-dependent viscosity (see Table 1). The left columns represent the structures of T (tone) and ψ (contour). The right columns represent the structures of isotherms (contour) and $\Phi/\Phi_{\rm ave}$ (tone) with common logarithm. The values of common logarithm of γ_v are shown at the left sides of the figures. Ra_s equals to 10^2 and the aspect ratio is fixed at one.

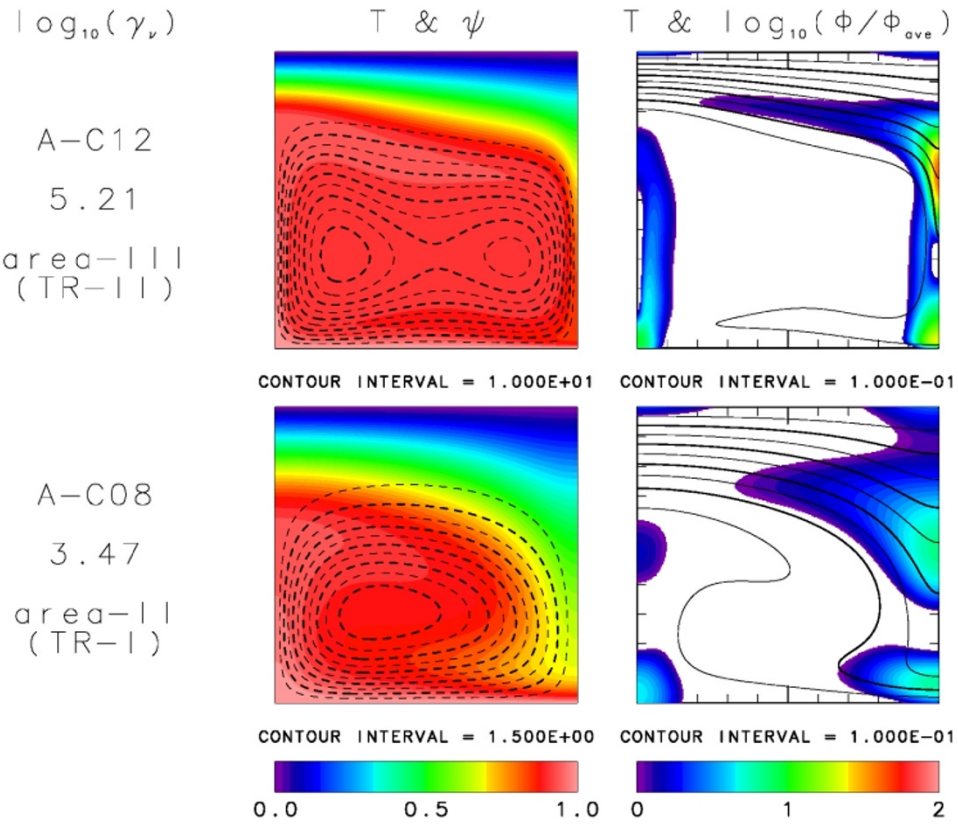

Fig. 3. As in Fig. 2, except for the predictions for models A-C12 and A-C08 (see Table 1).

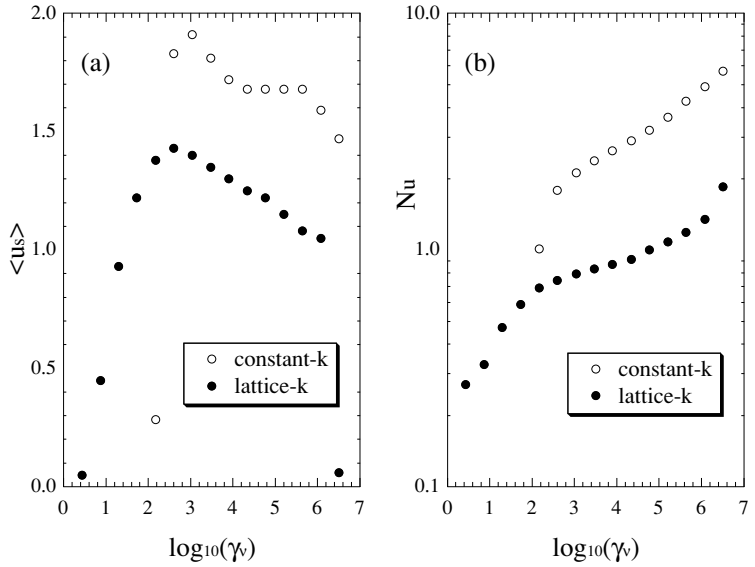

Fig. 4. Plots of $\langle u_s \rangle$ (a) and Nu (b) versus γ_v for models with lattice-k and constant-k, in which temperature-dependent viscosity is adopted. Ra_s equals to 10^2 and the aspect ratio is fixed at one. The open and solid circles indicate the cases with constant-k and lattice-k, respectively.

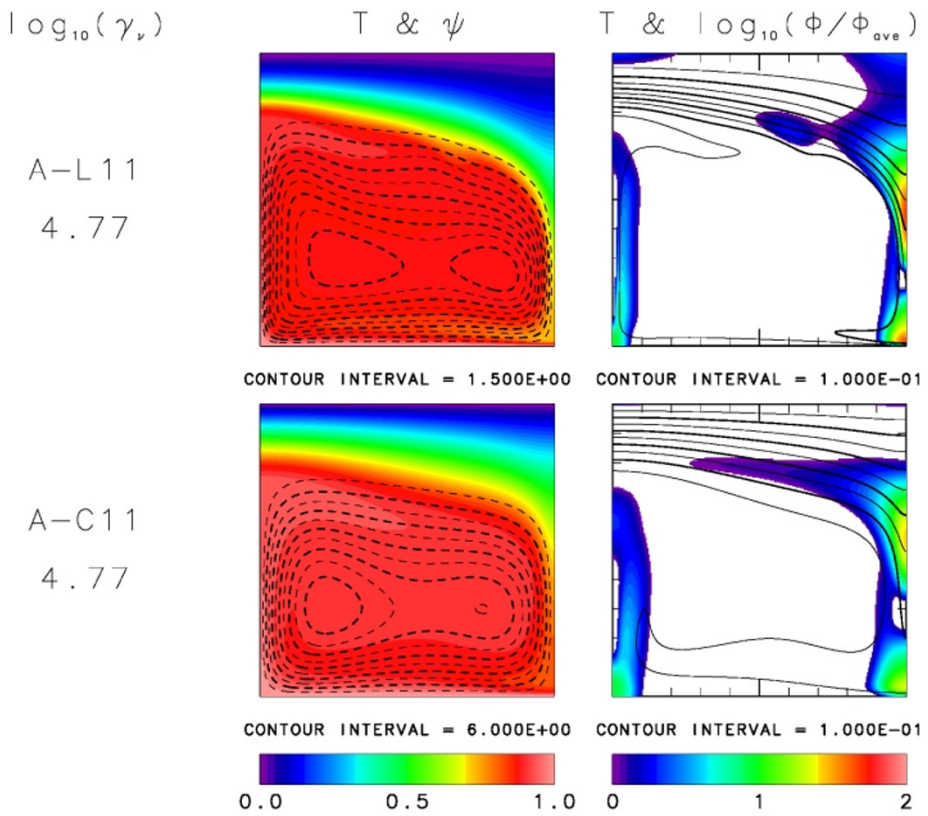

Fig. 5. As in Fig. 2, except for the predictions for models A-L11 (lattice-k) and A-C11 (constant-k) (see Table 1).

$\Phi/\Phi_{\rm ave}$ are expressed as follows,

$$\Phi = \tau_{ij}\frac{\partial u_i}{\partial x_j} = \frac{\nu(T)}{2}\left(\frac{\partial u_i}{\partial x_j} + \frac{\partial u_j}{\partial x_i}\right)^2 \quad (8)$$

$$\frac{\Phi}{\Phi_{\rm ave}} = \frac{\Phi}{\frac{1}{V}\oint_V \Phi dV} \quad (9)$$

where τ_{ij} is the shear stress, and V is the volume of the layer. A zone with a rate of viscous dissipation corresponds to the zone for a significant deformation caused by convective flows.

Figure 2 shows convective structures for models A-C14 and A-C06. In A-C06 for the area-I (Fig. 1), viscous dissipation takes on a maximum at the root of the downwelling (at $z = 0$), indicating no stiff-lid near the surface. Such a convective pattern is similar to that with a constant vis-

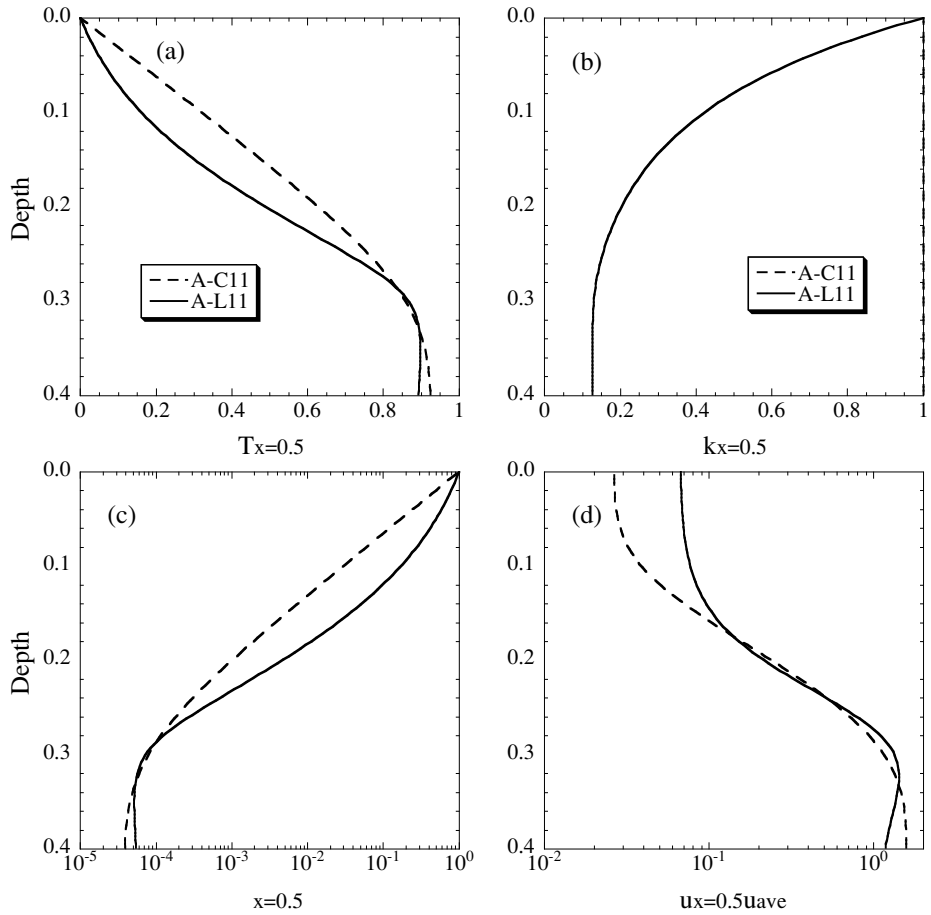

Fig. 6. Vertical profiles of T, k, ν and $u/u_{\rm ave}$. The index "$x = 0.5$" means that these values are estimated at the center of the convective cell. The solid and dashed lines represent cases A-L11 (lattice-k) and A-C11 (constant-k), respectively.

cosity, and is called as the small viscosity contrast (SVC) regime (Solomatov, 1995). In A-C14 for the area-IV, the viscous dissipation for the cold plume takes a maximum near the bottom of the upper TBL, and no viscous dissipation is predicted along the surface. In addition, small and isolated perturbations are predicted near the bottom of the upper TBL. This regime with a stiff-lid along the top is called as the stagnant-lid (ST) regime (Solomatov, 1995).

Figure 3 shows convective patterns for models A-C12 and A-C08. Cases A-C12 and A-C08 belong to the area-III (TR-II) and area-II (TR-I), respectively. In both cases, the viscous dissipation for the downwellings takes a maximum not at the surface but at the bottom of the upper TBL, and the significant viscous dissipation distributes vertically up to the surface (A-C08), or horizontally in the lowermost part of the upper TBL (A-C12). An isolated perturbation is not predicted around the bottom of the upper TBL. A less stiff-lid along the surface inferred from these results can be deformed and moved by a pull of the downwelling. Such convective patterns belong to the transitional (TR) regime (Solomatov, 1995).

The TR regime may be separated into two convective regimes. The difference between two regimes is obtained by comparing the model results for the area-II (A-C08) and the area-III (A-C12). For the area-II (A-C08), the viscous dissipation caused by the downwelling distributes vertically in the upper TBL. That is, the upper TBL can be deformed by the pull of the downwelling. This scenario looks like a formation of subduction zone. We call such a mode as the TR-I regime. For the area-III (A-C12), the viscous dissipation distributes horizontally in the lowermost part of the upper TBL. That is, the upper TBL is moved by the pull of the downwelling, rather than deformed as the area-II (A-C08). This looks like drift of plates without descending slabs. We call this mode as the TR-II regime.

The differences between the TR-I and the TR-II regimes can be also characterized by the different viscosity gradients in the upper TBLs as inferred from the temperature gradients shown in Fig. 3. Because the TR-II regime has a larger viscosity contrast between the top and bottom, the effective Rayleigh number becomes larger in the convective layer. In the upper TBL for the TR-II regime, therefore, its thickness becomes thinner and the viscosity gradient becomes steeper compared to those for the TR-I regime.

3.3 Influence of the lattice thermal conductivity on thermal convection with a shorter horizontal scale

In this section, we examine the effects of temperature-dependent lattice thermal conductivity (lattice-k defined by Eq. (4)) on thermal convection with the temperature-dependent viscosity, especially, on deformations of the upper TBL. The lattice thermal conductivity decreases with an increase of temperature.

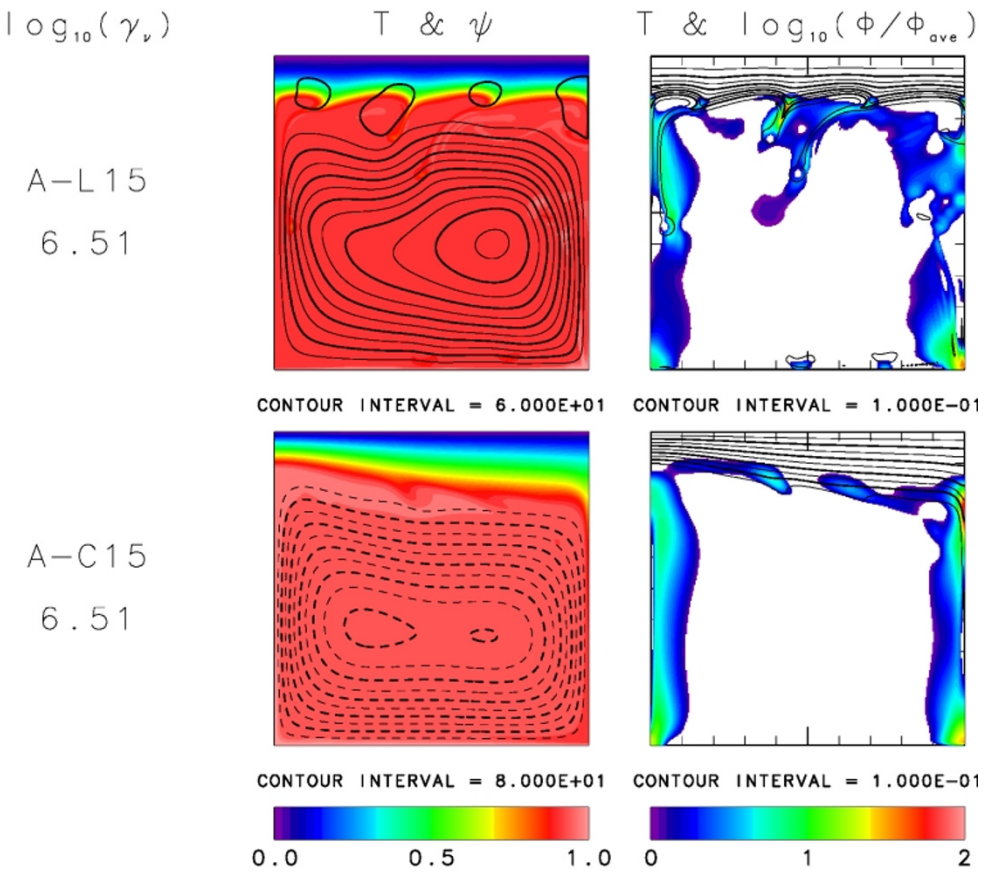

Fig. 7. As in Fig. 2 except for the predictions for models A-L15 (lattice-k) and A-C15 (constant-k) (see Table 1).

Figure 4 shows the plots of horizontal velocity at the top $\langle u_s \rangle$ and Nusselt number Nu versus the viscosity contrast across the layer, γ_v, to compare the results for constant-k and lattice-k models. The parameters for these numerical experiments are shown in Table 1. Values for $\langle u_s \rangle$ and Nu are lower for models with lattice-k except for the results of $\langle u_s \rangle$ with $\gamma_v = 10^{2.17}$. In models with $\gamma_v \sim 1$, thermal convection with constant-k has a small effective Rayleigh number, and fluid is almost motionless. On the other hand, the lattice-k increases an effective Rayleigh number, and fluid can flow even for $\gamma_v \sim 1$. The results for $\gamma_v > 10^{2.17}$ are consistent with those by Yanagawa *et al.* (2004), in which they obtained similar results based on a simple depth-dependent thermal conductivity model. They also found a physical meaning based on a loop model (Weinstein *et al.*, 1989) that the thermal convection for decreasing thermal conductivity with depth, similar to lattice-k here, weakens the heat transfer from the surface. A noticeable feature for the plots of $\langle u_s \rangle$ is the absence of the flat zone corresponding to the TR-II regime for constant-k. To understand why the TR-II regime disappears in models with lattice-k, we examine the convective structures for constant-k and lattice-k models.

Figure 5 shows convective structures for A-L11 and A-C11 with a viscosity contrast of $\gamma_v = 10^{4.77}$. In A-C11 with constant-k, the viscous dissipation for a cold plume distributes horizontally in the lower part of the upper TBL, and small and isolated disturbances are not predicted, corresponding to features characterizing the TR-II regime. In A-L11 with lattice-k, however, the viscous dissipation for a downwelling distributes vertically in the upper TBL, indicating a feature characterizing the TR-I mode. In addition, small and nearly isolated perturbation appears around the bottom. This is a feature characterizing the ST regime (see Fig. 2). That is, the convective regime for A-L11 has features common to both TR-I and ST regimes.

The temperature gradients in the upper TBL are different for models A-C11 and A-L11. That is, those for A-C11 are relatively constant compared with those for A-L11 (Fig. 5). Figure 6 shows the vertical profiles of temperature T, thermal conductivity k, viscosity v and normalized horizontal velocity $u/u_{\rm ave}$ for models shown in Fig. 5. The normalized horizontal velocity $u/u_{\rm ave}$ is defined by

$$\frac{u}{u_{\rm ave}} = \frac{u_{x=0.5}}{\frac{1}{V}\oint_V u dV} \tag{10}$$

The upper TBL for A-L11 is thinner than that for A-C11 because of an increase of effective Rayleigh number due to a decreasing lattice-k. The temperature gradient for A-C11 is almost linear. That for A-L11 is, however, gentler close to the surface and steeper close to the bottom of the upper TBL because the vertical heat flow must be kept constant in the TBL. The viscosity gradient also reflects the temperature gradient. In A-L11, the viscosity gradient is gentler close to the surface, consistent with the distribution of $u/u_{\rm ave}$ that the gradient of u/uave is gentler close to the surface. On the other hand, the viscosity gradient is steeper close to the bottom of the upper TBL, implying that the TBL is more

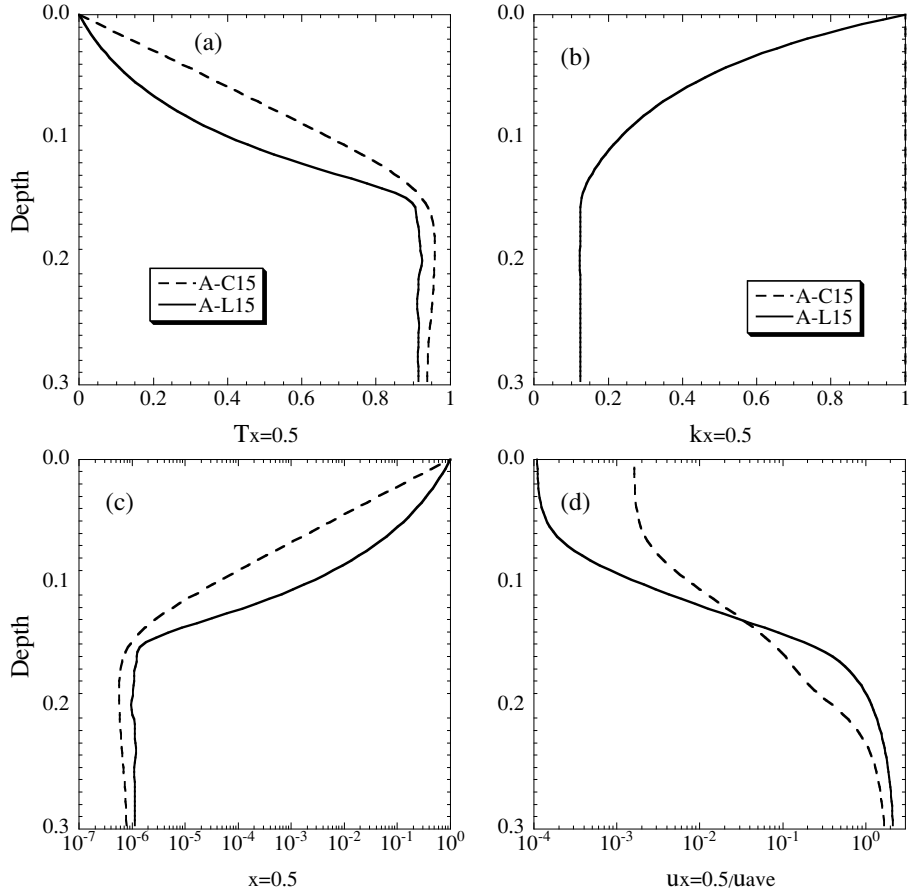

Fig. 8. As in Fig. 6, except for the predictions for models A-L15 (lattice-k) and A-C15 (constant-k) (see Table 1).

isolated dynamically from the underlying convective layer.

Predictions for A-L15 and A-C15 with $\gamma_\nu = 10^{6.51}$ belong to the ST regime (Fig. 7). The viscous dissipation distributes only in the lowermost part of the upper TBL, and small perturbations are predicted around the bottom. It is, however, clearly predicted for A-L15 that the scales of downwellings decrease and the number of cold plumes increases. A very steep temperature gradient is also predicted around the bottom of the upper TBL. This promotes its uppermost part to be stagnant. Figure 8 shows the vertical distributions of T, k, ν and $u/u_{\rm ave}$ to compare the model results for lattice-k (A-L15) and constant-k (A-C15). The same tendencies as those in Fig. 6 are predicted for A-L15, i.e. the thinner TBL, the gentler temperature gradient close to the surface and steeper temperature gradient around the bottom. As a result, viscosity gradient is also gentler close to the surface and steeper around the bottom. Too steep a viscosity gradient as predicted for A-L15 produces a dynamically isolated stagnant-lid along the surface. In other words, the pull of the downwelling cannot influence the deformation near the surface because the descending flows are decayed by a steeper viscosity gradient in the lower part of the thermal boundary layer, TBL. The narrower layer where $u/u_{\rm ave}$ changes rapidly indicates a more distinct boundary between the convective layer and isolated stagnant-lid. The differences for the TBLs between the constant-k and lattice-k models are mainly caused by (i) an increase of effective Rayleigh number due to a decreasing lattice-k and (ii) the temperature distribution due to a lattice-k with a constraint of constant vertical heat flux within the TBL.

Table 2. The list of numerical experiments with the aspect ratio fixed at two. The Rayleigh number estimated at the surface Ra_s equals to 10^2.

β in Eq. (3)	$\log_{10}(\gamma_\nu)$	constant-k	lattice-k
14	6.08	C-C14	C-L14
13	5.64	C-C13	C-L13
12	5.21	C-C12	C-L12
11	4.77	C-C11	C-L11
10	4.34	C-C10	C-L10
9	3.90	C-C09	C-L09
8	3.47	C-C08	C-L08
7	3.04	C-C07	C-L07
6	2.6	C-C06	C-L06
5	2.17	C-C05	C-L05
4	1.73	C-C04	none

3.4 Influence of the lattice thermal conductivity on thermal convection with a longer horizontal scale

A less-developed upper TBL, predicted for models with a relatively small γ_ν, does not prevent fluid from being cooled. Thermal convection with a relatively large γ_ν has a large effective Rayleigh number at the bottom of the convecting region, resulting in an efficiency of heat transfer.

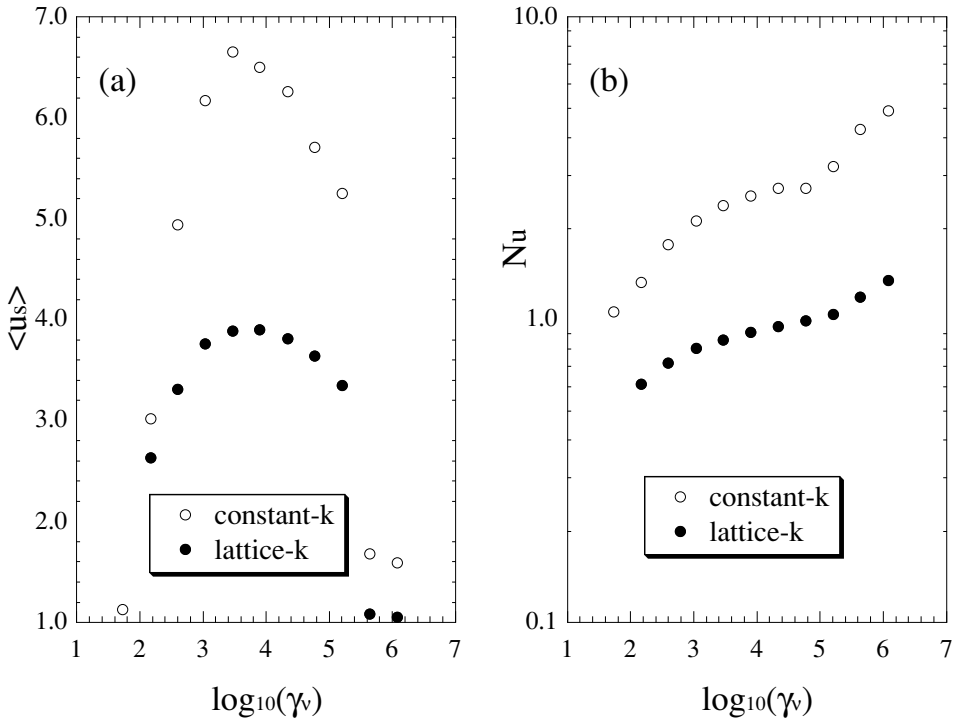

Fig. 9. Plots of $\langle u_s \rangle$ (a) and Nu (b) versus γ_v for models with lattice-k and constant-k, in which temperature-dependent viscosity is adopted. Ra_s equals to 10^2 and the aspect ratio is fixed at two. The open and solid circles indicate the cases with constant-k and lattice-k, respectively.

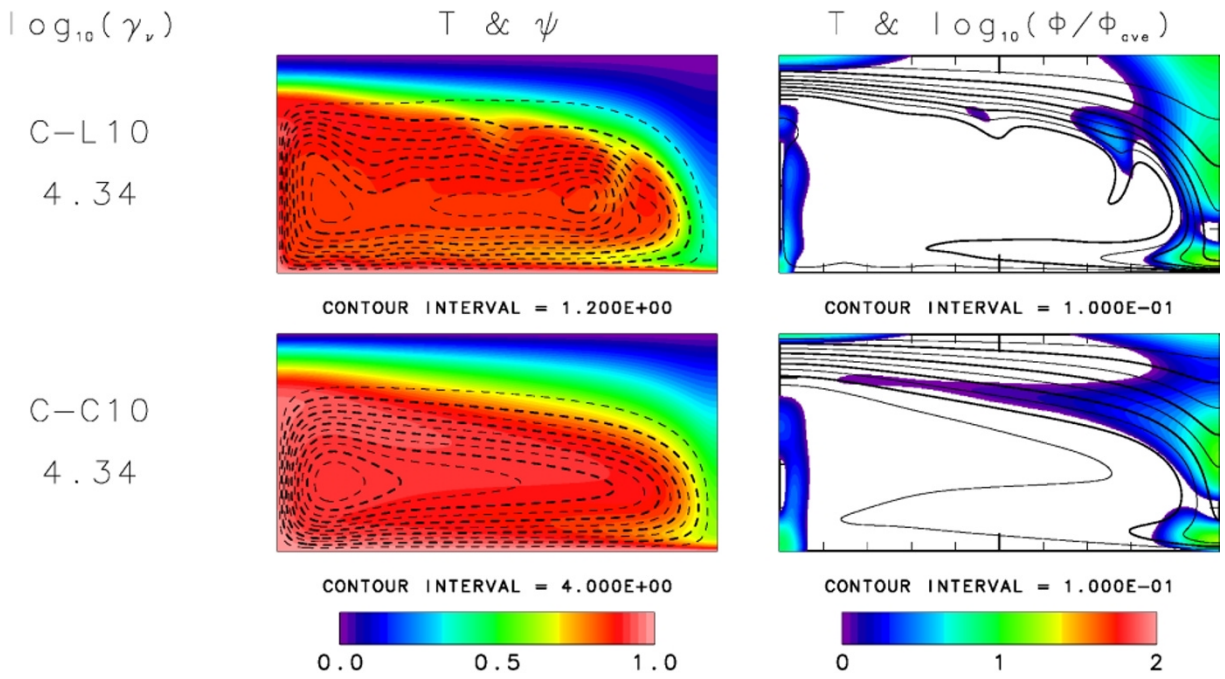

Fig. 10. Two-dimensional structures of T, ψ and $\Phi/\Phi_{\rm ave}$ for models with lattice-k (C-L10) and constant-k (C-C10) (see Table 2), in which temperature-dependent viscosity is adopted. The left columns represent the structures of T (tone) and Ψ (contour). The right columns represent the structures of isotherms (contour) and $\Phi/\Phi_{\rm ave}$ (tone) with common logarithm. The values of common logarithm of $\Phi/\Phi_{\rm ave}$ are shown at the left sides of the figures. Ra_s equals to 102 and the aspect ratio is fixed at two.

Therefore, the horizontal scale of such convection does not become longer, because the fluid can be cooled enough, while the fluid flows along the surface. However, a cold and thick TBL at the surface, with a very high γ_v, prevents fluid from being cooled. Therefore, a long horizontal scale is required for cooling and descending downwards. In fact, aspect ratio of convective cell in the Earth's mantle is probably larger than one, and therefore studies of thermal convection with a longer horizontal scale are required to understand the dynamics of the Erath. Other types of physics,

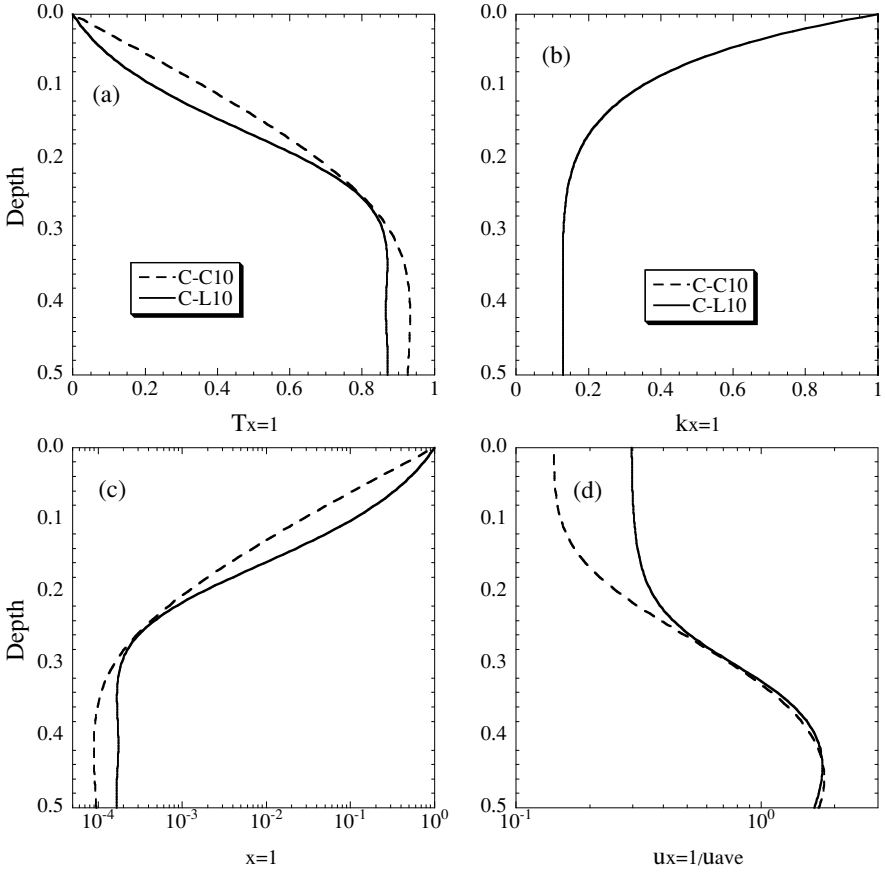

Fig. 11. Vertical profiles of T, k, ν and $u/u_{\rm ave}$. The index "$x = 1$" means that these values are estimated at the center of the convective cell. The solid and dashed lines represent cases C-L10 (lattice-k) and C-C10 (constant-k), respectively.

such as depth-dependent viscosity and thermal expansivity also drive the flow to longer wavelengths.

To study structures of thermal convection with a longer horizontal scale, we adopt the box with aspect ratio fixed at two. The horizontal velocity at the surface $\langle u_s \rangle$ and Nusselt number Nu versus the viscosity contrast γ_ν are shown in Fig. 9 for models with aspect ratio with two. These results are also consistent with the results using a simple depth-dependent thermal conductivity model (Yanagawa *et al.*, 2004). The parameters for these numerical experiments are shown in Table 2. The results for $\langle u_s \rangle$ with constant-k indicate three convective regimes, i.e. the SVC ($\gamma_\nu \leq 10^{3.04}$), the TR ($10^{3.47} \leq \gamma_\nu \leq 10^{4.34}$) and the ST regimes ($\gamma_\nu \leq 10^{4.77}$). It is, however, impossible to separate the TR regime into the TR-I and TR-II regimes. In thermal convection with a longer horizontal scale, the cold plume becomes stronger because the fluid is sufficiently cooled while the fluid flows along the surface. This extends the TR-I regime to a larger viscosity contrast, resulting in the vanishment of the TR-II. In the plot of the $\langle u_s \rangle$ with lattice-k, however, differences between these boundaries become less clear because of a stronger pull by the downwelling associated with the lattice-k convection.

Figure 10 depicts the convective structures with $\gamma_\nu = 10^{4.34}$. In C-C10 with constant-k, the viscous dissipation distributes both horizontally along the bottom of the upper TBL and vertically for the downwelling. That is, the convective structure has features characterized by both the TR-I and TR-II regimes predicted for an aspect ratio of unity. In C-L10 with lattice-k, the viscous dissipation for the cold plume takes a maximum at the bottom of the downwelling and the significant viscous dissipation distributes vertically up to the surface. These convective features are characterized by the TR-I regime. In addition, there are small disturbances around the lower part of the upper TBL as characterized by the ST regime. Figure 11 shows the vertical profiles of T, k, ν and $u/u_{\rm ave}$ of the models shown in Fig. 10. These results are consistent with those with aspect ratio fixed at unity.

Figure 12 shows the convective structures with $\gamma_\nu = 10^{5.21}$. In C-C12, viscous dissipation for a cold plume takes a maximum at the bottom of the upper TBL. In addition, a small and isolated perturbation appears at the bottom, consistent with the ST mode. The structure for C-C12 is called as an elongated-ST regime by Kameyama and Ogawa (2000). The elongated-ST regime is the ST regime with a longer horizontal scale. In C-L12, a significant viscous dissipation for the downwelling distributes vertically in the upper TBL as characterized by the TR-I regime. In addition, small and isolated disturbances are predicted around the lower part of the upper TBL as predicted for the ST regime. That is, such a convective structure with lattice-k has features characterizing both the TR-I and ST regimes in models with the aspect ratio of unity. The structure for C-L12 belongs to the TR regime for convective structure with a longer horizontal scale found by Kameyama and Ogawa

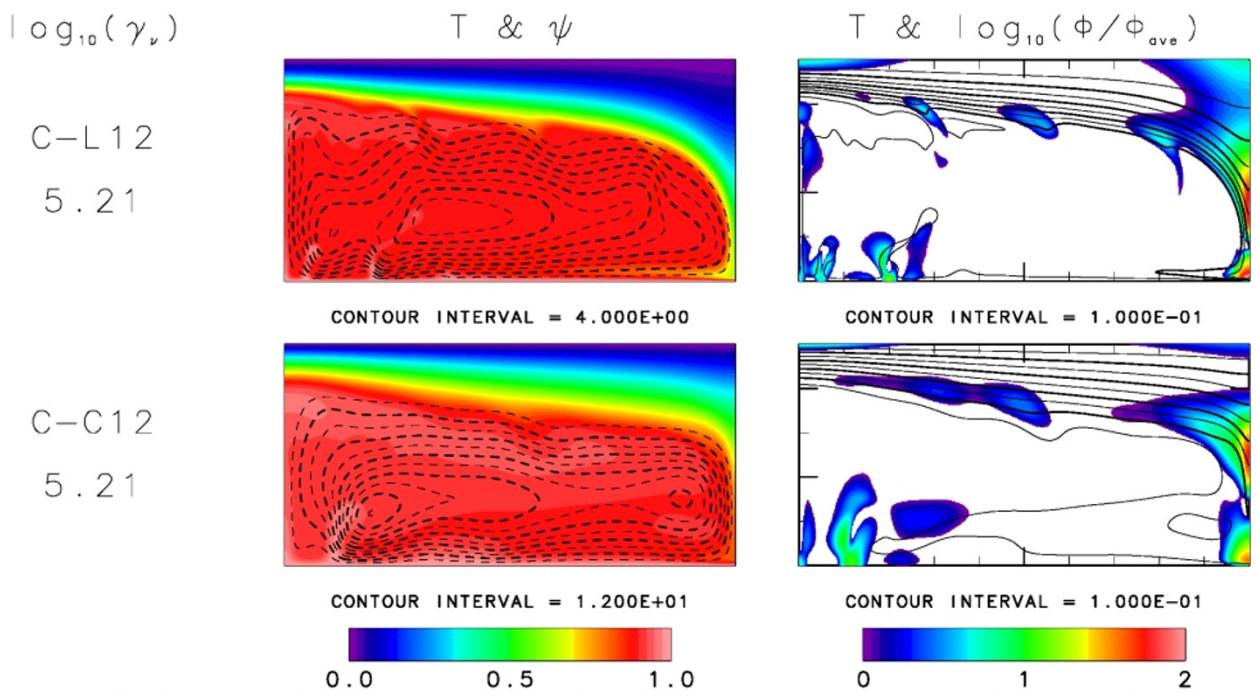

Fig. 12. As in Fig. 10 except for the predictions for models C-L12 (lattice-k) and C-C12 (constant-k) (see Table 2).

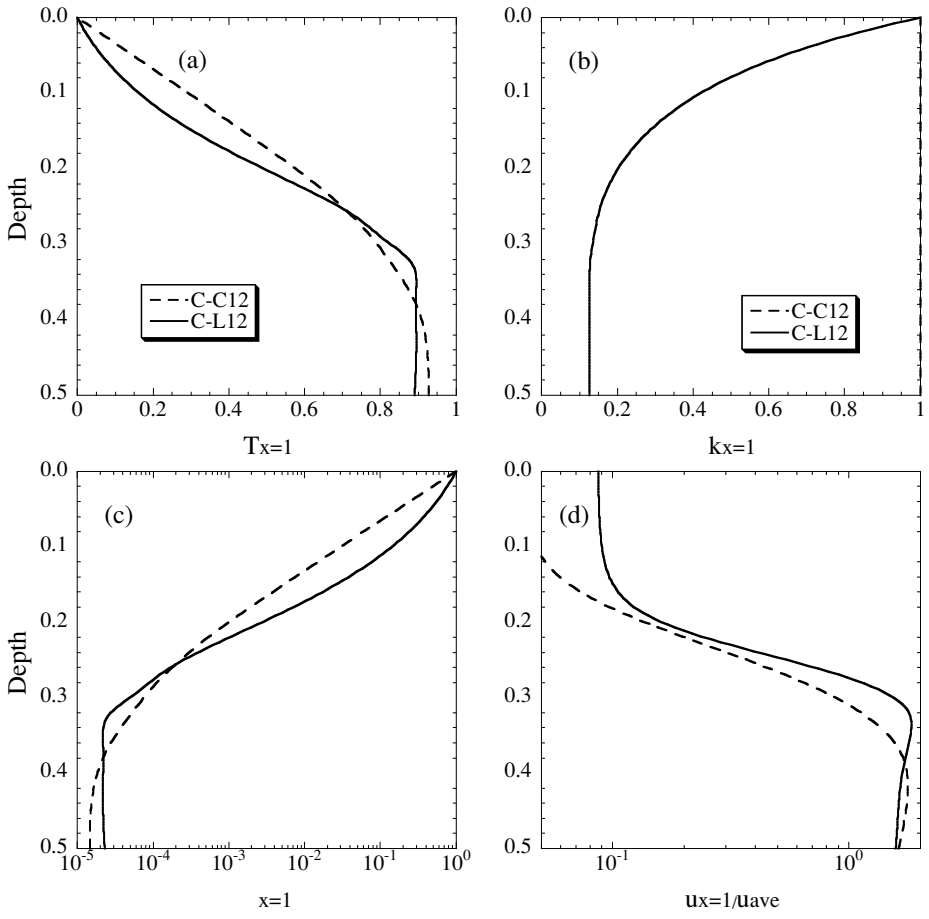

Fig. 13. As in Fig. 11, except for the predictions for models C-L12 (lattice-k) and C-C12 (constant-k) (see Table 2).

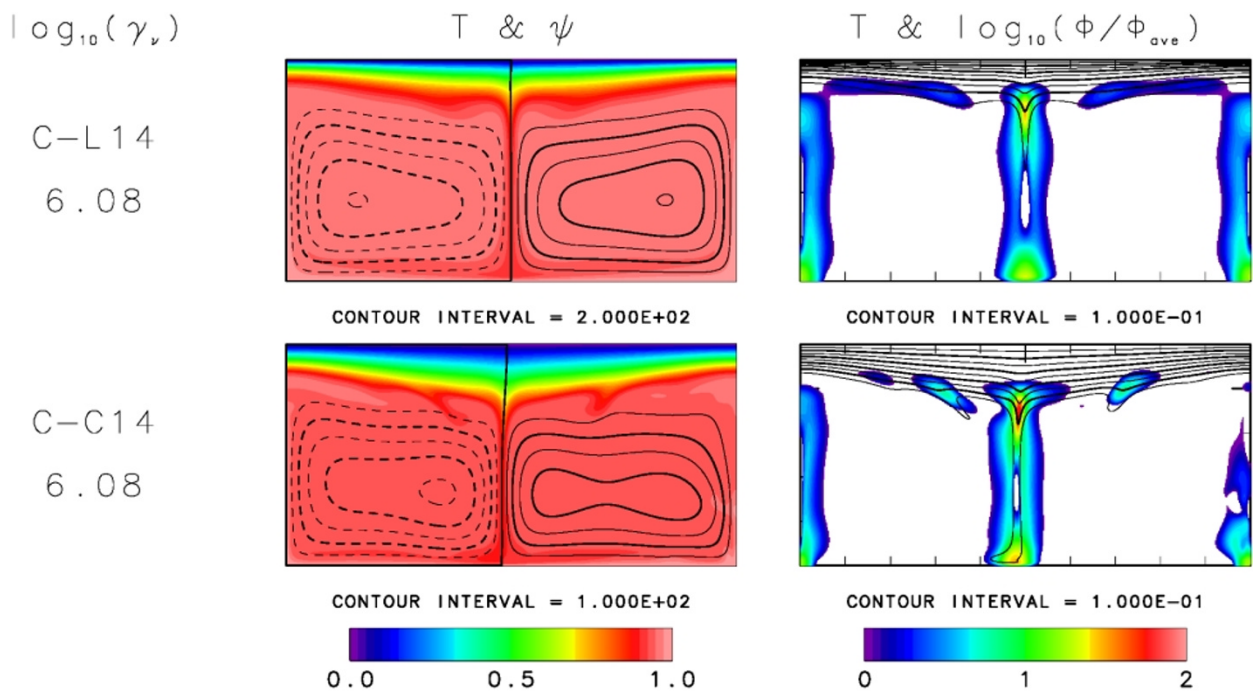

Fig. 14. As in Fig. 10 except for the predictions for models C-L14 (lattice-k) and C-C14 (constant-k) (see Table 2).

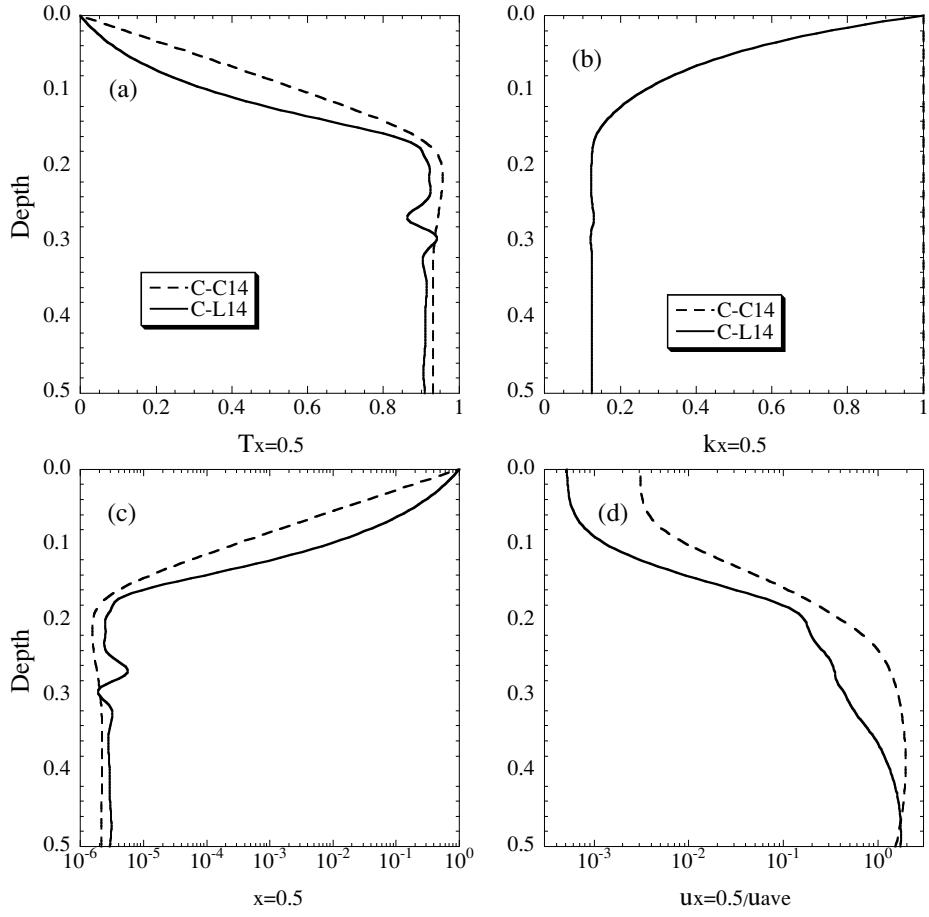

Fig. 15. As in Fig. 11, except for the predictions for models C-L14 (lattice-k) and C-C14 (constant-k) (see Table 2).

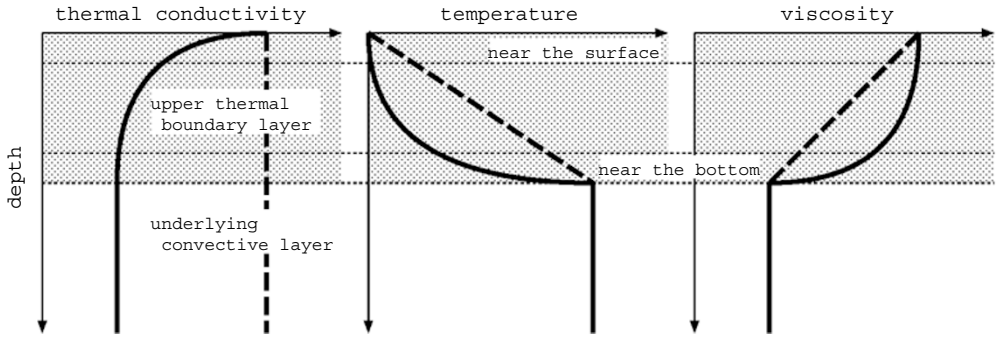

Fig. 16. Schematic vertical profiles of thermal conductivity, temperature and viscosity for models with lattice-k and constant-k. Solid and dashed lines indicate profiles with lattice-k and constant-k, respectively.

(2000). The vertical distributions of T, k, ν and $u/u_{\rm ave}$ for models shown in Fig. 12 are depicted in Fig. 13. The differences between the constant-k and lattice-k are also consistent with those with aspect ratio fixed at one.

Figure 14 shows the results for a viscosity contrast associated $\gamma_\nu = 10^{6.08}$. In both C-L14 and C-C14, no viscous dissipation is predicted along the surface. That is, the convective regime for both cases belongs to the ST regime. The aspect ratio of convective cells becomes shorter than two, consistent with the previous results that the convection for the ST regime with $\gamma_\nu > 10^6$ has a smaller horizontal scale than constant viscosity convection (e.g. Weinstein and Christensen, 1991; Tackley, 1993; Ratcliff *et al.*, 1997; Kameyama and Ogawa, 2000). Small-scale disturbances around the lower part of the TBL predicted for lattice-k are attributed to an increase of effective Rayleigh number associated with a decrease of lattice thermal conductivity with depth. This tendency is also seen in Fig. 7. The vertical distributions of T, k, ν and $u/u_{\rm ave}$ for these models are depicted in Fig. 15. A thinner and dynamically more isolated stagnant-lid is clearly indicated for thermal convection with lattice-k.

4. Discussion and Concluding Remarks

Up to now, thermal convection with a temperature-dependent viscosity and constant thermal conductivity (constant-k) has extensively been studied, and previous works have indicated three convective regimes dependent on the viscosity contrast γ_ν, i.e. the small viscosity contrast (SVC), the transitional (TR) and the stagnant-lid (ST) regimes (Solomatov, 1995; Moresi and Solomatov, 1995; Solomatov and Moresi, 1997). Kameyama and Ogawa (2000) proposed an additional convective regime, i.e. an elongated-ST regime characterized by the convective structure with a longer stiff-lid along the surface. In this study, we mainly examined the effects of the temperature-dependent thermal conductivity (lattice-k) on thermal convection with temperature-dependent viscosity.

The thermal convection with lattice-k has a lower temperature and slower convective flow, consistent with the results based on a depth-dependent thermal conductivity model by Yanagawa *et al.* (2004). In particular, effects of the lattice-k are emphasized for convective structure with a stiff-lid predicted for very high viscosity contrast. That is, the upper TBL is more cooled because of the higher value of lattice-k close to the surface. The decreasing lattice-k with depth increases an effective Rayleigh number, and the convection becomes more vigorous. As a result, the TBL becomes thinner and its temperature gradient also becomes steeper. These causes are summarized in Subsection 3.3.

Figure 16 shows schematic vertical distributions of thermal conductivity, temperature and viscosity around the upper TBL. For models with temperature-dependent lattice thermal conductivity, the temperature gradient is gentler close to the surface and is steeper around the bottom of TBL. Because the viscosity is controlled by the distribution of temperature, the viscosity gradient is gentler close to the surface and is steeper in the lowermost part of the TBL. The diffusion term of momentum includes the term proportional to the viscosity gradient. Here we emphasize that the vertical viscosity gradient across the lithosphere is more important than the value of the viscosity itself. That is, the convective flow is decayed rapidly across the layer with a steeper viscosity gradient. In the lowermost part of the TBL with lattice-k, the pulls by the cold plumes are decayed because of the steeper viscosity gradient. Such a part promotes the lid to be separated from the underlying convective layer. In addition, small and isolated perturbations appear around the bottom of the thermal boundary layer, because the local Rayleigh number increases due to the steeper temperature gradient, the low viscosity and the low thermal conductivity. Therefore the TBL becomes thinner than that for the constant-k.

The surface deformation of the lid is less sensitive to the weaker pulls by the smaller descending plumes, but much sensitive to the stronger pulls by larger downwellings. In the lowermost part of the lid with a sharp viscosity gradient, weaker pulls by small downwellings are diffused before they drive fluid near the top. On the other hand, stronger pulls by larger downwellings survive the diffusion there and then pull down the fluid near the surface (Regenauer-Lieb and Yuen, 1998). In the upper part of the lid with an almost constant viscosity, these downward pulls, which survive in the lowermost part, can easily drive fluid at the top. Such a situation may be valid for plate tectonics on the Earth, especially, for the determination of the site for subduction initiation.

Other planets, for example, Mercury, Venus and Mars, have surface deformations with various scales, and some of them may be related to viscous flows inside the plan-

ets. Venus has mantle convection producing some kinds of tectonic features. However, there is no plate tectonics on Venus, and therefore mantle flow must produce surface deformations by propagating stresses across the thick lithosphere (Kaula, 1990; Kidder and Phillips, 1996; Hansen *et al*., 1997). The scales of surface deformations may depend on the scales of underlying viscous flows and the degree of the viscosity gradient in the lowermost part of the lithosphere. That is, the lattice component of temperature-dependent thermal conductivity may promote the deformations of the surface by decreasing viscosity contrast near the surface of the lithosphere. The deformations on the surface of Mars (Zuber, 2001) may be explained by the same arguments posed for Venus.

Not only mantle rocks but also ice have a strong temperature-dependent rheology (Hobbs, 1974; Echelmeyer and Kamb, 1986). Some of the Galilean Satellites, for example, Europa, Ganymede and Callisto are covered by icy shells (Deschamps and Sotin, 2001). Europa and Ganymede have very thick icy shells (several hundreds of kilometers) and deformations with various scales have been observed on their surfaces (McKinnon, 1997; McKinnon, 1999). Ice has also a rather strong temperature-dependence in thermal conductivity (Hooke, 1998). Because the effects of lattice-k on temperature-dependent rheology are more significant in the regions with a lower temperature, it may efficiently promote deformations with smaller scales on icy surfaces of the Galilean Satellites (Schenk *et al*., 2001).

Acknowledgments. The authors wish to thank Paul J. Tackley and Masaki Ogawa for constructive and helpful reviews. The numerical calculations were performed on the Fujitsu VPP5000 Supercomputer in the data processing center of the National Astronomical Observatory of Japan. This research is supported by the geophysics and CSEDI programs of the National Science Foundation.

References

Arakawa, A., Computational design for long-term numerical integrations of the equations of atmospheric motion, *Comput. Phys*., **1**, 119–143, 1966.

Christensen, U. R., Heat transport by variable viscosity convection and implications for the Earth's thermal evolution, *Phys. Earth Planet. Int*., **35**, 264–282, 1984.

Clark, S. P., Radiative transfer in the Earth's mantle, *Trans. AGU*, **38**, 931–938, 1957.

Deschamps, F. and C. Sotin, Thermal convection in the outer shell of large icy satellites, *J. Geophys. Res*., **106**, 5107–5121, 2001.

Dubuffet, F. and D. A. Yuen, A thick pipe-like heat-transfer mechanism in the mantle: nonlinear coupling between 3-D convection and variable thermal conductivity, *Geophys. Res. Lett*., **27**, 17–20, 2000a.

Dubuffet, F., D. A. Yuen, and M. Rabinowicz, Effects of a realistic mantle thermal conductivity on the patterns of 3D convection, *Earth Planet. Sci. Lett*., **171**, 401–409, 1999.

Dubuffet, F., D. A. Yuen, and T. K. B. Yanagawa, Feedback effects of variable thermal conductivity on the cold downwellings in high Rayleigh number convection, *Geophys. Res. Lett*., **27**, 2981–2984, 2000b.

Dubuffet, F., D. A. Yuen, and E. S. G. Rainey, Controlling thermal chaos in the mantle by positive feedback from radiative thermal conductivity, *Nonlinear Process. Geophys*., **129**, 359–375, 2002.

Echelmeyer, K. and B. Kamb, Rheology of ice II and ice III from high-pressure extrusion, *Geophys. Res. Lett*., **13**, 693–696, 1986.

Frank-Kamenetskii, D. A., *Diffusion and Heat Transfer in Chemical Kinetics*, Plenum, New York, 1969.

Fujisawa, H., N. Fujii, H. Mizutani, H. Kanamori, and S. Akimoto, Thermal diffusivity of Mg_2SiO_4, Fe_2SiO_4 and NaCl at high pressures and temperature, *J. Geophys. Res*., **73**, 4727–4733, 1968.

Hansen, V. L., J. J. Willis, and W. B. Banerdt, Tectonic overview and synthesis, in *Venus II*, The University of Arizona Press, Arizona, 1997.

Hobbs, P.V., *Ice Physics*, Clarendon Press, Oxford, England, 1974.

Hofmeister, A., Mantle values of thermal conductivity and the geotherm from phonon lifetimes, *Science*, **283**, 1699–1706, 1999.

Hofmeister, A., Thermal conductivity of spinels and olivines from vibrational spectroscopy: Ambient conditions, *American Mineralogist*, **86**, 1188–1208, 2001.

Hooke, R. Leb., *Principles of Glacier Mechanics*, Prentice Hall, 1998.

Kameyama, M. and M. Ogawa, Transitions in thermal convection with strongly temperature-dependent viscosity in a wide box, *Earth Planet. Sci. Lett*., **180**, 355–367, 2000.

Kanamori, H., N. Fujii, and H. Mizutani, Thermal diffusivity measurement of rock-forming minerals from 300 to 1100 K, *J. Geophys. Res*., **73**, 595–605, 1968.

Kaula, W. M., Mantle convection and crustal evolution on Venus, *Geophys. Res. Lett*., **17**, 1401–1403, 1990.

Kidder, J. G. and R. J. Phillips, Convection-driven subsolidus crustal thickening on Venus, *J. Geophys. Res*., **101**, 23181–23194, 1996.

McKinnon, W. B., Sighting the seas of Europa, *Nature*, **386**, 765–767, 1997.

McKinnon, W. B., Convective instability in Europa's floating ice shell, *Geophys. Res. Lett*., **26**, 951–954, 1999.

Moresi, L. N. and V. S. Solomatov, Numerical investigation of 2D convection with extremely large viscosity variations, *Phys. Fluid*., **7**, 2154–2162, 1995.

Ratcliff, J. T., P. J. Tackley, G. Schubert, and A. Zebib, Transitions in thermal convection with strongly variable viscosity, *Phys. Earth Planet. Int*., **102**, 201–212, 1997.

Regenauer-Lieb, K. and D. A. Yuen, Rapid convection of elastic energy into plastic shear heating during incipient necking of the lithosphere, *Geophys. Res. Lett*., **25**, 2737–2740, 1998.

Schatz, J. F. and G. Simmons, Thermal conductivity of Earth materials at high temperatures, *J. Geophys. Res*., **77**, 6966–6983, 1972.

Schenk, P. M., W. B. McKinnon, D. Gwynn, and J. M. Moore, Flooding of Ganymede's bright terrains by low-viscosity water-ice lavas, *Nature*, **410**, 57–60, 2001.

Schubert, G., D. L. Turcotte, and P. Olson, *Mantle Convection in the Earth and Planets*, Cambridge University Press, Cambridge, 2001.

Solomatov, V. S., Scaling of temperature- and stress-dependent viscosity convection, *Phys. Fluids*., **7**, 266–274, 1995.

Solomatov, V. S. and L. N. Moresi, Three regimes of mantle convection with non-Newtonian viscosity and stagnant lid convection on the terrestrial planets, *Geophys. Res. Lett*., **24**, 1907–1910, 1997.

Tackley, P. J., Effects of strongly temperature-dependent viscosity on time-dependent, 3-dimensional models of mantle convection, *Geophys. Res. Lett*., **20**, 2187–2190, 1993.

Tatebe, O., The Multigrid Preconditioned Conjugate Gradient Method, Proceedings of Sixth Copper Mountain Conference on Multigrid Methods, NASA Conference Publication, 3224, 621–634, 1993.

van den Berg, A. P., D. A. Yuen, and V. Steinbach, The effects of variable thermal conductivity on mantle heat transfer, *Geophys. Res. Lett*., **28**, 575–578, 2001.

van den Berg, A. P., D. A. Yuen, and J. R. Allwardt, Nonlinear effects from variable thermal conductivity and mantle internal heating: Implications for massive melting and secular cooling of mantle, *Phys. Earth Planet. Inter.*, **129**, 359–375, 2002a.

van den Berg, A. P. and D. A. Yuen, Delayed cooling of the Earth's mantle due to variable thermal conductivity and the formation of a low conductivity zone, *Earth Planet. Sci. Lett*., **199**, 403–413, 2002b.

Weinstein, S. A. and U. Christensen, Convection planforms in a fluid with a temperature-dependent viscosity beneath a stress-free upper boundary, *Geophys. Res. Lett*., **18**, 2035–2038, 1991.

Weinstein, S. A., P. L. Olson, and D. A. Yuen, Time-dependent large aspect-ratio thermal convection in the Earth's mantle, *Geophys. Astrophys. Fluid Dyn*., **47**, 157–197, 1989.

Yanagawa, T. K. B., M. Nakada, and D. A. Yuen, A simplified mantle convection model for thermal conductivity stratification, *Phys. Earth Planet. Int*., **146**, 163–177, 2004.

Zuber, M. T., The crust and mantle of Mars, *Nature*, **412**, 220–227, 2001.

T. K. B. Yanagawa, M. Nakada, and D. A. Yuen (e-mail: davey@krissy.geo.umn.edu)